Photoacoustics 38 (2024) 100626

Contents lists available at ScienceDirect

Photoacoustics

journal homepage: www.elsevier.com/locate/pacs

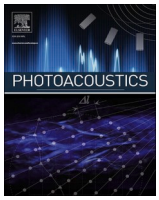

High-sensitivity narrow-band T-shaped cantilever Fabry-perot acoustic sensor for photoacoustic spectroscopy

Jilong Wang [a,1], Qiaoyun Wang [a,b,*,1], Chongyue Yan [a], Shunyuan Xu [a], Xin Zou [a], Qiang Wu [c], Wai Pang Ng [c], Richard Binns [c], Yong-Qing Fu [c]

[a] College of Information Science and Engineering, Northeastern University, Shenyang, Liaoning Province 110819, China
[b] Hebei Key Laboratory of Micro-Nano Precision Optical Sensing and Measurement Technology, Qinhuangdao 066004, China
[c] Faculty of Engineering & Environment, Northumbria University, Newcastle upon Tyne NE1 8ST, UK

ARTICLE INFO

Keywords:
Fiber-optic acoustic sensor
Fabry-Perot sensor
T-shaped cantilever
Photoacoustic spectroscopy
Acetylene detection

ABSTRACT

Photoacoustic spectroscopy (PAS) has been rapidly developed and applied to different detection scenarios. The acoustic pressure detection is an important part in the PAS system. In this paper, an ultrahigh sensitivity Fabry-Perot acoustic sensor with a T-shaped cantilever was proposed. To achieve the best acoustic pressure effect, the dimension of the cantilever structure was designed and optimized by finite element analysis using COMSOL Multiphysics. Simulation results showed that the sensitivity of such T-shaped cantilever was 1.5 times higher than that based on a rectangular cantilever, and the resonance frequency of T-shaped cantilever were able to modulate from 800 Hz to 1500 Hz by adjusting the multi-parameter characteristics. Experimental sensing results showed that the resonance frequency of T-shaped Fabry-Perot acoustic sensor was 1080 Hz, yielding a high sensitivity of 1.428 μm/Pa, with a signal-to-noise ratio (SNR) of 84.8 dB and a detectable pressure limit of 1.9 $\mu Pa/Hz^{1/2}$@1 kHz. We successfully used such acoustic sensor to measure acetylene (C_2H_2) concentration in the PAS. The sensitivity of PAS for C_2H_2 gas was 3.22 pm/ppm with a concentration range of 50 ppm ~100 ppm, and the minimum detection limit was 24.91ppb.

1. Introduction

Acoustic sensing has many applications in various areas including environmental monitoring [1–3], industrial process control [4,5], photoacoustic (PA) spectroscopy (PAS) [6–13], and sound source location [14]. The conventional electronic acoustic sensors (EAS) were widely used for acoustic wave detection due to their advantages of good frequency responses and high fidelity over a wide frequency range. However, EAS did not work well in harsh environments because of the weak anti-electromagnetic interference (EMI) [15,16]. Therefore, acoustic sensors with a high sensitivity, passive nature, and narrow bandwidth are required in the PAS detection system[17–22]. Fabry-Perot (F-P) acoustic sensors had been considered an excellent choice due to their small size, high sensitivity, passive nature, immunity to EMI, cost-effectiveness and safety features [23–31]. Different types of diaphragm materials are applied for F-P sensors. Xiang *et al.* [32] presented an F-P sensor based on fiber-optic collimation and a gold diaphragm of 140 nm thick. The minimum detectable sound pressure (MDP) level was 95.3 $\mu Pa/Hz^{1/2}$ at 2 kHz, and the flat response frequency range was 400–12 kHz. Sekip *et al.* [33] proposed a diaphragm-type transducer using cellulose triacetate and achieved a SNR of 72.20 dB at 103.16 mPa sound pressure, and the MDP was 17.91 $\mu Pa/Hz^{1/2}$ at 2 kHz. Sun *et al.* [34] utilized an electrostatic spinning technique to fabricate a diaphragm by assembling a composite film consisting of polyvinyl alcohol (PVA) and cellulose nanocrystals (CNCs). The acoustic pressure response was 1.89 V/Pa at 16.2 kHz, which was surpassed those of devices using pure polymer membranes. The sensitivity of the F-P acoustic sensor could also be improved by changing the diaphragm structure, such as flat diaphragm, corrugated diaphragm, drilled diaphragm, and cantilever [35–39]. Niu *et al.* [40] introduced a F-P transducer based on a slotted diaphragm, which was capable to balancing the sensitivity and resonant frequency. The F-P transducer's sound pressure sensitivity at 2 kHz was 37.44 mV/Pa, approximately double that of a pure circular membrane under the same conditions. Qi *et al.* [41] suggested a sensor with a flywheel-shaped sensitive diaphragm, which overcame the sensitivity limitations of the edge-fixed circular structures. The

* Corresponding author at: College of Information Science and Engineering, Northeastern University, Shenyang, Liaoning Province 110819, China.
E-mail address: wangqiaoyun@neuq.edu.cn (Q. Wang).
[1] Jilong Wang and Qiaoyun Wang contribute equally to this work

https://doi.org/10.1016/j.pacs.2024.100626
Received 16 April 2024; Received in revised form 3 June 2024; Accepted 3 June 2024
Available online 8 June 2024

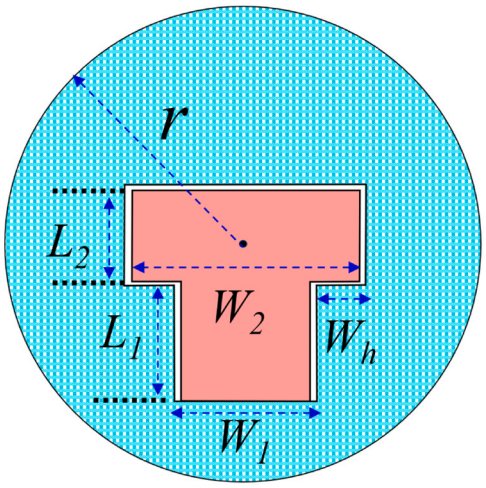

Fig. 1. The schematic diagram of T-shaped cantilever structure.

sensitivity at 4.5 kHz was 1.525 nm/Pa, and the MDP was 13.06 μPa/Hz$^{1/2}$. The F-P sensors were widely used in photoacoustic spectroscopy gas detection systems [42–49]. Jiao *et al.* proposed a spherical photoacoustic cell combined with a photoacoustic sensor for detecting methane gas, the minimum detection limit (MDL) measured within an average time of 1000 seconds is 126.9 ppb. The system was applicable for trace gas detection which needed remote and long-distance. Guo *et al.* [50] introduced an ultra-high sensitivity F-P sensor utilizing a silicon cantilever to improve the gas detection, achieving a sound pressure sensitivity of 1.753 μm/Pa at 1 kHz and an MDP of 0.21 μPa/Hz$^{1/2}$. However, due to the simple structure of these traditional cantilevers, it was difficult to achieve a high-sensitivity acoustic detection while matching the resonance frequency of F-P sensor and the resonance frequency of PA cell.

In this paper, an ultrahigh sensitivity fiber-optic acoustic sensor based on T-shaped cantilever (**FOTCS**) was proposed. The F-P cavity was formed by the end face of fiber and inner surface of T-shaped cantilever. To improve sensitivity of such the **FOTCS**, the vibration characteristics and dimensions of T-shaped cantilever were analyzed and optimized using finite element analysis (FEA). Finally, the **FOTCS** was used in PAS for C_2H_2 gas detection. Both simulation and experimental studies showed that this structure had a high sensitivity in narrow-band frequency, and it is suitable for the sound pressure detection in the PAS.

2. Theoretical analysis and simulation

The structure of the T-shaped cantilever was shown in the Fig. 1. The whole T-shaped structure mainly consisted of two cantilever segments spliced horizontally and vertically. The sensitivity and resonance frequency of the cantilever were affected by the dimensions of its different parts, including the length and width of the vertical cantilever (L_1 *and* W_1), the length and width of the horizontal cantilever (L_2 *and* W_2), and the thickness of the membrane (H).

Accordance to the Euler-Bernoulli beam theory, the deflection equation of the cantilever is as follows [51]:

$$\frac{d^2y(x)}{dx^2} = -\frac{M(x)}{EI} \tag{1}$$

where $y(x)$ is the cantilever's deformation at position x, $M(x)$ is its bending moment at position x, E is its elastic modulus, and I is its moment of inertia across its cross-section. The bending moments and the section moments of the two parts can be written as follows [52]:

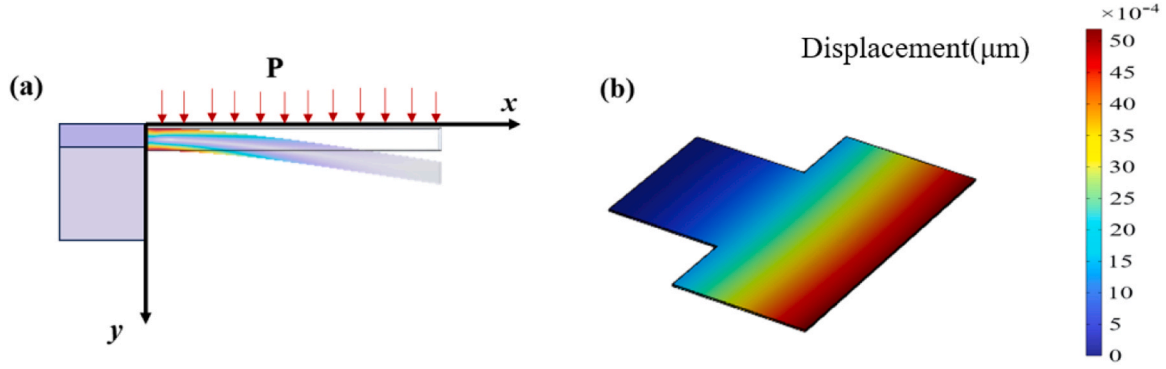

Fig. 2. (a) Bending deflection analysis of the T-shaped cantilever. (b) Displacement analysis of the T-shaped cantilever based on COMSOL.

Table 1
Comparison of resonance frequencies of different shaped cantilevers.

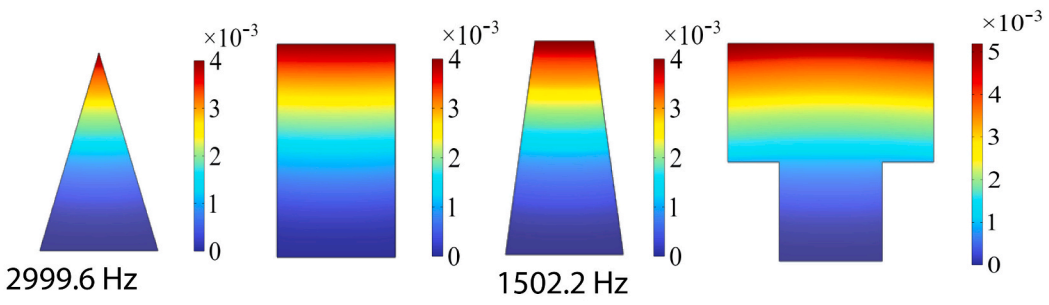

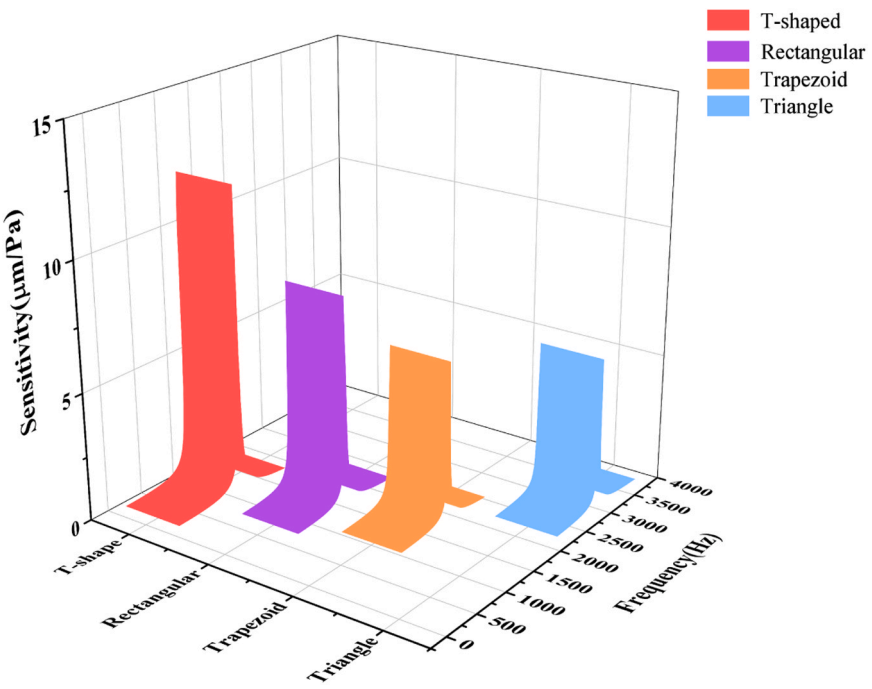

Fig. 3. Frequency response based on four different shapes of cantilevers (T-shaped, rectangular, trapezoid, triangle) under the same total length.

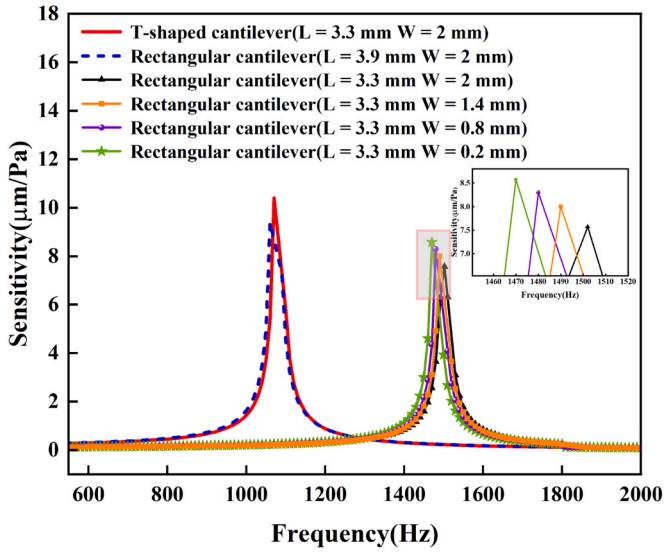

Fig. 4. Comparison of frequency response and sensitivity of T-shaped and rectangular cantilever with the same length or same resonant frequency.

$$M(x)=\begin{cases} M(1)=\frac{1}{2}W_1P(L_1-x)^2+\frac{1}{2}W_2PL_2\left[2\left(L_1-x\right)+L_2\right) & (0\le x\le L_1) \\ M(2)=\frac{1}{2}PW_2(L_1+L_2-x)^2 & (L_1\le x\le L_1+L_2) \end{cases} \tag{2}$$

$$I(x)=\begin{cases} \frac{W_1h^2}{12} & (0\le x\le L_1) \\ \frac{W_2h^3}{12} & (L_1\le x\le L_2) \end{cases} \tag{3}$$

where P is the sound pressure exerted onto the membrane, L_1 and L_2 are the lengths and the transverse of the cantilever, I_1 and I_2 are the inertia of the two cross sections. W_1 and W_2 are the width of the starting cantilever segment, and the width of the transverse beam segment. The boundary condition of the structure and the middle joint can be expressed as:

$$\frac{dy(0)}{dx}=0 \tag{4}$$

$$y(0)=0 \tag{5}$$

Accordingly, the deflection expressions of the two parts can be derived as follows:

$$y_1(x)|_{(0\le x\le L_1)}=\frac{P}{2EW_1h^3}\left(6\left(W_1{L_1}^2+2L_1L_2W_2+W_2{L_2}^2\right)x^2-4\left(W_1L_1+W_2L_2\right)x^3+W_1x^4\right) \tag{6}$$

$$y_2(x)|_{(L_1\le x\le L_2)}=\frac{P}{2EW_1h^3}\left(W_1x^4-4W_1\left(L_1+L_2\right)x^3+6W_1(L_1+L_2)^2x^2+12\left(L_1+L_2\right)L_1L_2\left(W_2-W_1\right)x+L_1L_2\left(W_1-W_2\right)\left(4{L_1}^2+6L_1L_2\right)-W_1{L_1}^4\right) \tag{7}$$

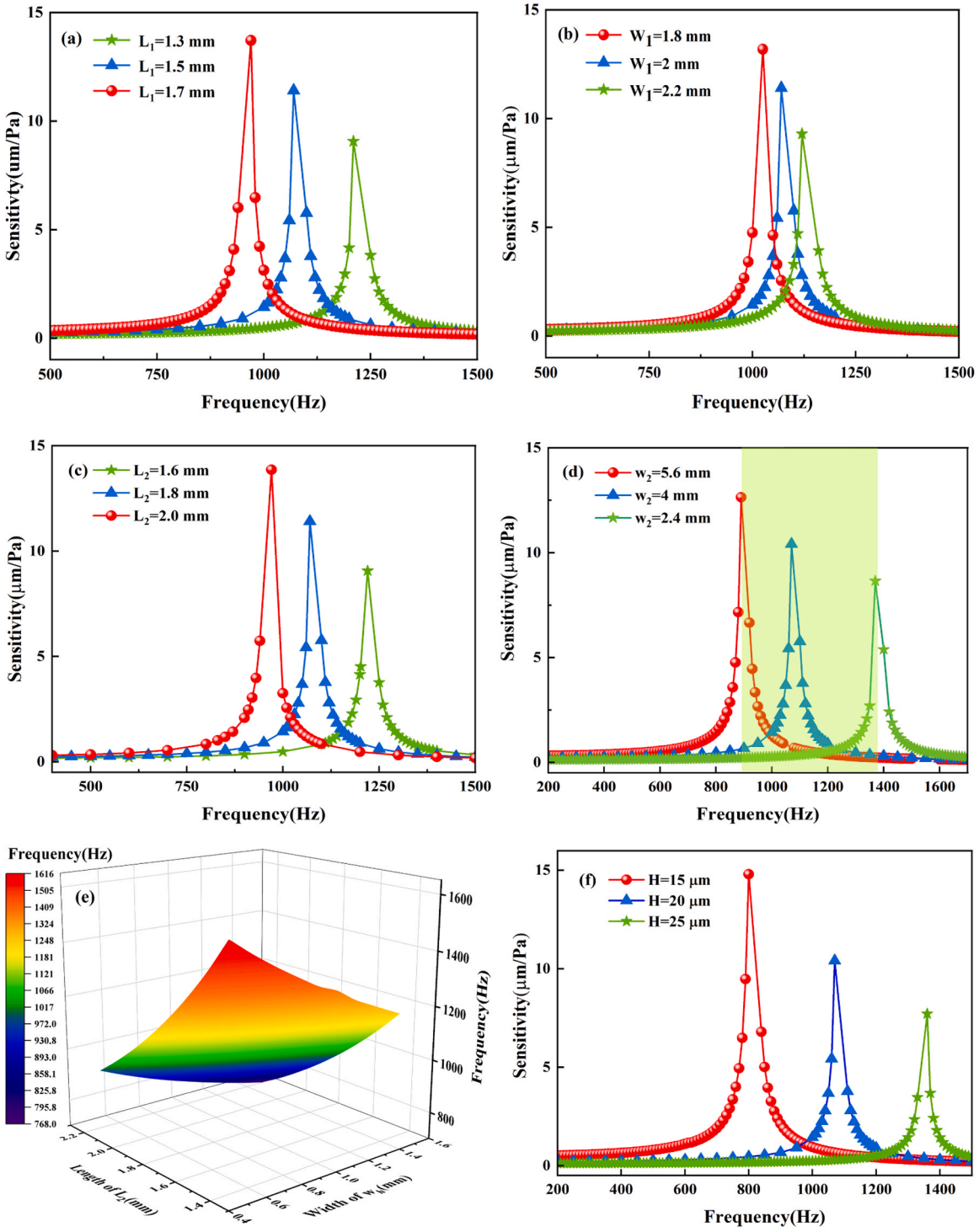

Fig. 5. Finite element analysis based on COMSOL. (a)The relationships between the frequency response of **FOTCS** and the length of the L_1. (b)The width of the W_1.(c) The length of the L_2.(d) The width of the W_2. (e)Trend of resonance frequency with the length of L_2 and the width of W_h.(f)Thickness of the T-shaped cantilever.

When investigating structural vibrations, it is crucial to consider the stiffness coefficients of two sections of the T-shaped cantilever, which can be assumed as the spring constants. The overall stiffness coefficient (k) of the T-shaped cantilever can be expressed as the sum of the spring constant (k_c) of the beam, and the supplementary spring constant (k_a) due to the surrounding air. Therefore, the stiffness coefficient k of the T-shaped cantilever can be expressed as [50]:

$$k = k_c + k_a = \frac{P(W_1L_1 + W_2L_2)}{d} + \frac{2\kappa {A_c}^2 F}{5V_a} \tag{8}$$

where $\kappa$is the heat ratio, A_c is the area of the cantilever, V_a is the volume of the displaced air. The maximum deformation at the end of the structure is shown as:

$$y|_{\max} = y(x = L_1 + L_2) \tag{9}$$

when the total spring constant and mass of the system's vibration are given, the complete frequency response $A(\omega)$ can be expressed as follows [53]:

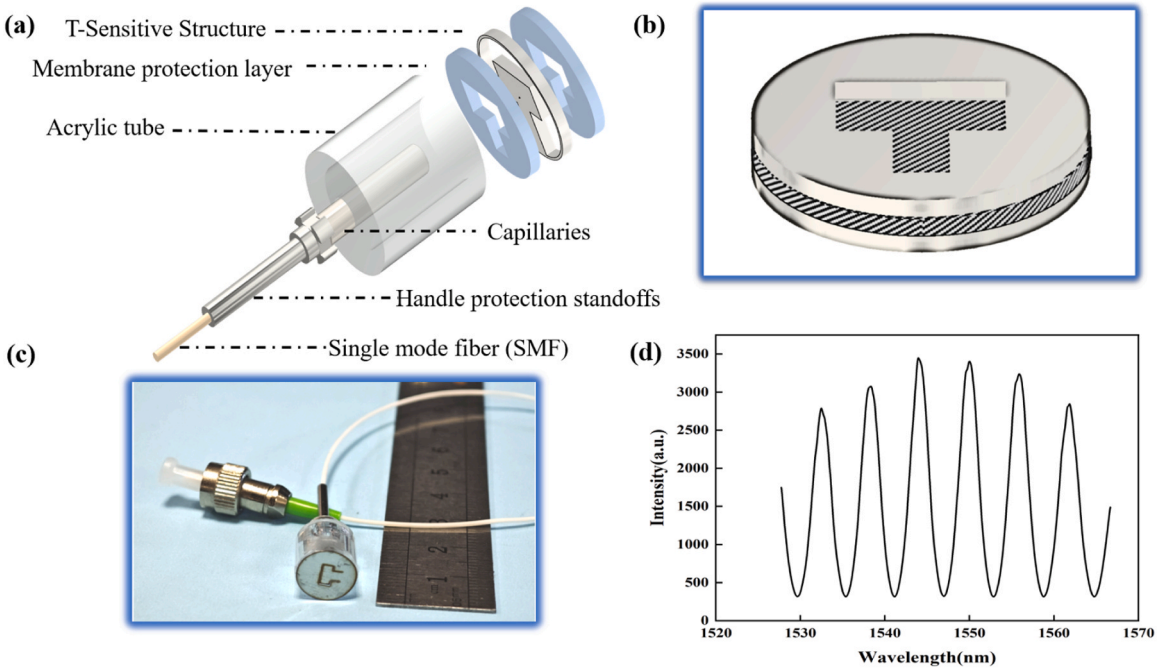

Fig. 6. (a) Acrylic tubes nested in each other model drawing. (b) The three-layer package of the sensing head. (c) **FOTCS** imaged by a camera. (d) Interference spectrum of **FOTCS**.

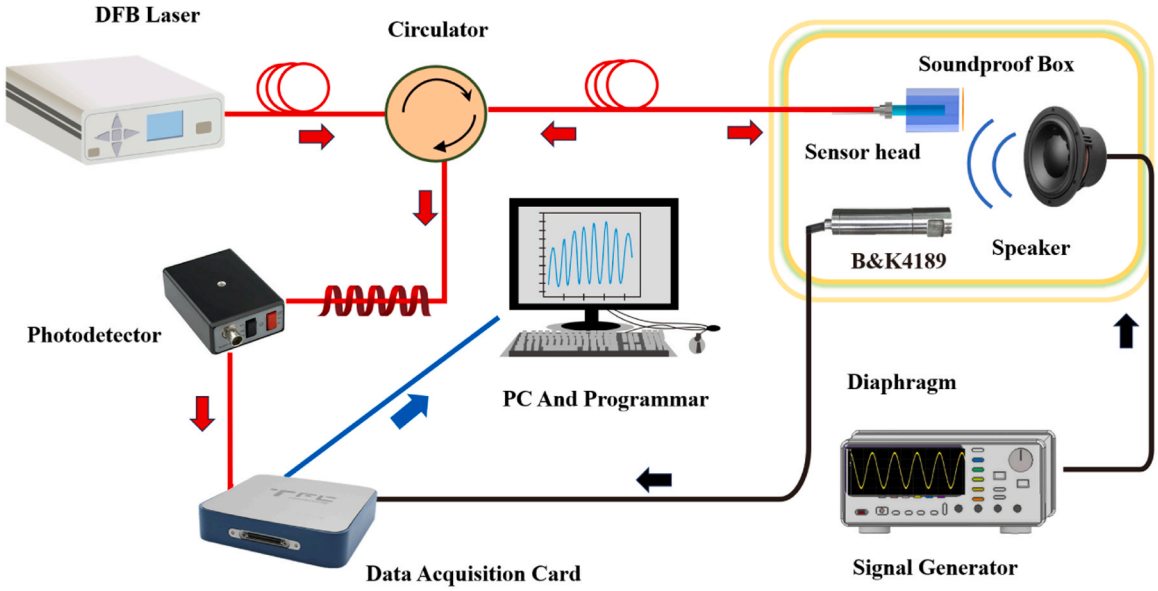

Fig. 7. Sensors Experimental system construction diagram.

$$f_o = \frac{1}{2\pi}\sqrt{\frac{k}{m_{eff}}} \tag{10}$$

$$A(\omega) = \frac{P}{m\sqrt{\left(\omega_0^2 - \omega^2\right)^2 + \left(\omega\beta/m\right)}} \tag{11}$$

where f_0 is the resonance frequency, m_{eff} is the effective mass of the T-shaped cantilever, ω_0 is the first resonant angular frequency, ω is the angular frequency, and β is the damping coefficient of acoustic wave in air. Finite element analysis (FEA) was used to show the response performance of the cantilever. When the uniform pressure is loaded on the T-shaped cantilever, the deformation of the cantilever simulated according to Eq.9 can be obtained and the results are shown in Fig. 2. The maximum deformation was at the end of the T-shaped cantilever. To get the maximum variation of the cavity length, the F-P cavity can be formed by the fiber's end face and the end inner surface of the T-shaped cantilever. According to Eq. 12, we can obtain the intensity of the interferometric spectrum of the sensor based on the variation in cavity length, and subsequently the magnitude of the external acoustic pressure during demodulation can be obtained based on the length of the chamber [53].

$$I(\lambda) = 2I_0(\lambda)\left[1 + \gamma\cos\left(\frac{4\pi(d_0 + y_2)}{\lambda} + \pi\right)\right] \tag{12}$$

where $I_0(\lambda)$ represents the spectrum of incident light, d_0 represents the

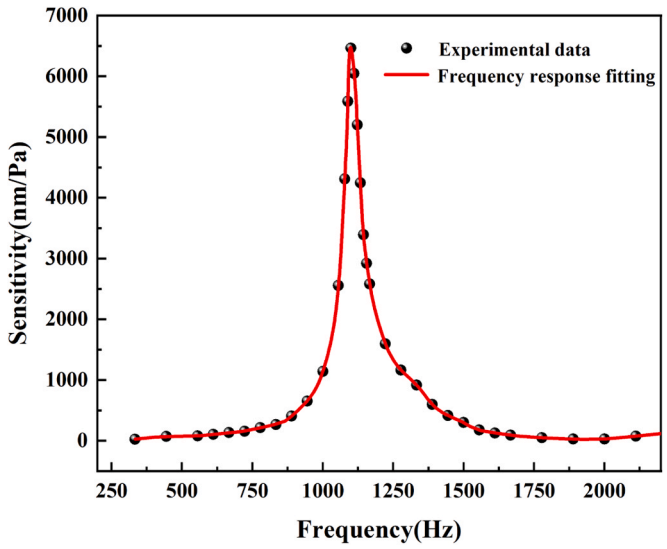

Fig. 8. Frequency response spectrum of the **FOTCS**.

static cavity length of the F-P and γ is the cavity stripe fineness.

The common F-P acoustic sensor mainly adopted flat diaphragm [36] or rectangular cantilever [50]. In order to improve the sensitivity of F-P acoustic sensor, we study the structure of the diaphragm. Triangular, trapezoidal, rectangular and T-shaped cantilevers were common cantilever types [54], so we chose these four shapes for comparison simulation. To reflect the differences brought about by the different shapes, we tried to ensure that the total length and initial width of each cantilever were the same, the resonance frequencies can be obtained as listed in Table 1. It can be seen that the resonance frequency of the T-shaped structure is the lowest. The frequency of photoacoustic gas detection was mainly determined by the resonance photoacoustic cell, generally the resonance frequency of the resonance photoacoustic cell was in the range of 1000 Hz ~2000 Hz [55,56].

The sensitivities of the different shaped cantilever at their resonance frequencies were simulated, and the obtained results are shown in Fig. 3. It showed that the sensitivity of the sensor with the T-shaped cantilever was higher than those of other shaped cantilevers. These results showed that the **FOTCS** had a much better advantage in the lower frequency range. The resonant frequency and sensitivities comparison when the T-shaped cantilever and rectangular cantilever had the same length or the same resonant frequency were shown in Fig. 4. When the length of cantilever was constant, the width of the rectangular cantilever was adjusted within the range of 0.2 mm to 2 mm, the resonant frequency of rectangular cantilever was increased with the decreasing width of rectangular cantilever, and the sensitivity of rectangular cantilever was decreased the decreasing width of rectangular cantilever. For the same length, the T-shaped cantilever's sensitivity was 10.6 μm/Pa and the rectangular's was 7.4 μm/Pa. When the resonant frequencies of T-shaped and rectangular cantilever were the same, the length of rectangular cantilever was 3.9 mm, and its sensitivity was slightly lower than that of the T-shaped cantilever. However, the optical fiber end face was aligned with the rectangular cantilever of length at 3.3 mm, the sensitivity at this position was 7.5 μm/Pa, and the sensitivity of T-shaped cantilever was about 1.4 times higher than that of rectangular cantilever. These results demonstrated that sensitivity of T-shaped cantilever was higher than that of the rectangular cantilever.

To study the sensitivity changes of the **FOTCS**, we performed the optimization analysis of the dimensional parameters of the cantilever. The initial part of the T-shaped cantilever was a simple rectangle, and the effects of L_1 and W_1 were shown in Fig. 5**(a)** and **(b)**. The sizes determined after optimization were 1.5 mm and 2 mm respectively. Fig. 5**(c)** showed the frequency responses as the length of cantilever is 1.6 mm, 1.8 mm, and 2 mm, respectively. The simulation results showed that the resonance frequency was decreased and the sensitivity was increased when the length of L_2 was increased. In order to keep the resonance frequency near 1 kHz for being compatible with the PA cell, we chose 1.8 mm as the final length. When the width of the horizonal cantilever was increased, the resonance frequency of the T-shaped cantilever was decreased, and the sensitivity was increased as shown in Fig. 5**(d)**. The width of the horizontal(W_2) section can be changed by adjusting the width of the turning section (W_h). These results were quite different from those of the rectangular cantilever, because the resonance frequency of rectangular cantilever was insensitive to the changes of width. The green area in the Fig. 5**(d)** represented the range of resonance frequencies by changing the width of the horizonal cantilever. The resonance frequency was changed from 800 Hz to 1500 Hz when the width of W_2 is changed from 2.4 mm to 4 mm. The resonance frequency of the **FOTCS** can be easily matched with that of the PA cell by changing the width of W_2. In this paper, W_2 was fixed at 4 mm. The influences of length and width of the transverse beam segment on the resonance frequencies can be observed by a three-dimensional plot as shown in Fig. 5**(e).** The projection on the XOY plane showed a broader spectrum of frequency space within such the size-optimized framework, facilitating precise adjustment of resonance frequencies to meet specific requirements. Fig. 5**(f)** showed the trend of resonance frequency with thickness. The sensitivity of the T-shaped cantilever was decreased but its resonant frequency was increased with the increase of its thickness. In this paper, the thickness of the stainless steel was fixed at 20 μm, thus the conventional rectangular cantilever has only two single attributes, i.e., length and width. When the resonance frequency of such rectangular cantilever was gradually adjusted by dimensions, the frequency range which can be adjusted is very small, and thus there are some issues such as required excessively long lengths and complicated manufacturing process. Therefore, the T-shaped cantilever we developed in this study has great advantages to achieve a much wider resonance frequency range because of its special geometry designs.

In the final design, lengths of such two cantilever segments in the vertical and horizontal directions of T-shaped structure are 1.5 mm and 1.8 mm, respectively, whereas their corresponding widths are 2 mm and 4 mm, respectively. The simulation results clearly indicated that by optimizing the parameters of the T-shaped cantilever structure, we can achieve a wide resonance frequency range to match the desired working frequency of the PA cell.

3. Results and discussion

The designed **FOTCS** set-up was composed by a single mode fiber (SMF), glass tubes and a T-shaped cantilever, as shown in Fig. 6**(a)**. We used a laser marking machine to etch out T-shaped cantilever on a stainless steel diaphragm with a 5 μm gap between the cantilever and the frame. Its effect on the frequency response was equivalent to a high-pass filter [57].At micrometer scale, the effect on cantilever vibration performance was negligible. Three types of glass tubes with different diameters embedded within each other were used in this work to meet the dimensions required by the PAS. The outer diameter and inner diameter of the outermost tubes were 10 mm and 6 mm, respectively. The diaphragm was attached to the surface of the outermost tube, and the structure was shown in Fig. 6**(b)**. The circular diaphragm with a T-shaped cantilever was etched out of a stainless-steel diaphragm with thickness of 100 μm using a laser beam cutting process. The L_1, W_1, L_2, W_2, H of the T-shaped cantilever were 1.5 mm, 2 mm, 1.8 mm, 4 mm, 20 μm, respectively. The assembled acoustic sensor was shown in Fig. 6**(c)**. The T-shaped cantilever and the T-shaped penetrated hole were positioned parallel to each other and the diaphragms with a T-shaped through hole were used to clamp the diaphragm with the T-shaped cantilever for supporting. The T-shaped cantilever could vibrate freely. Such a designed set-up not only prevents the possible collapse and nonlinear responses of the diaphragm, but also improves the

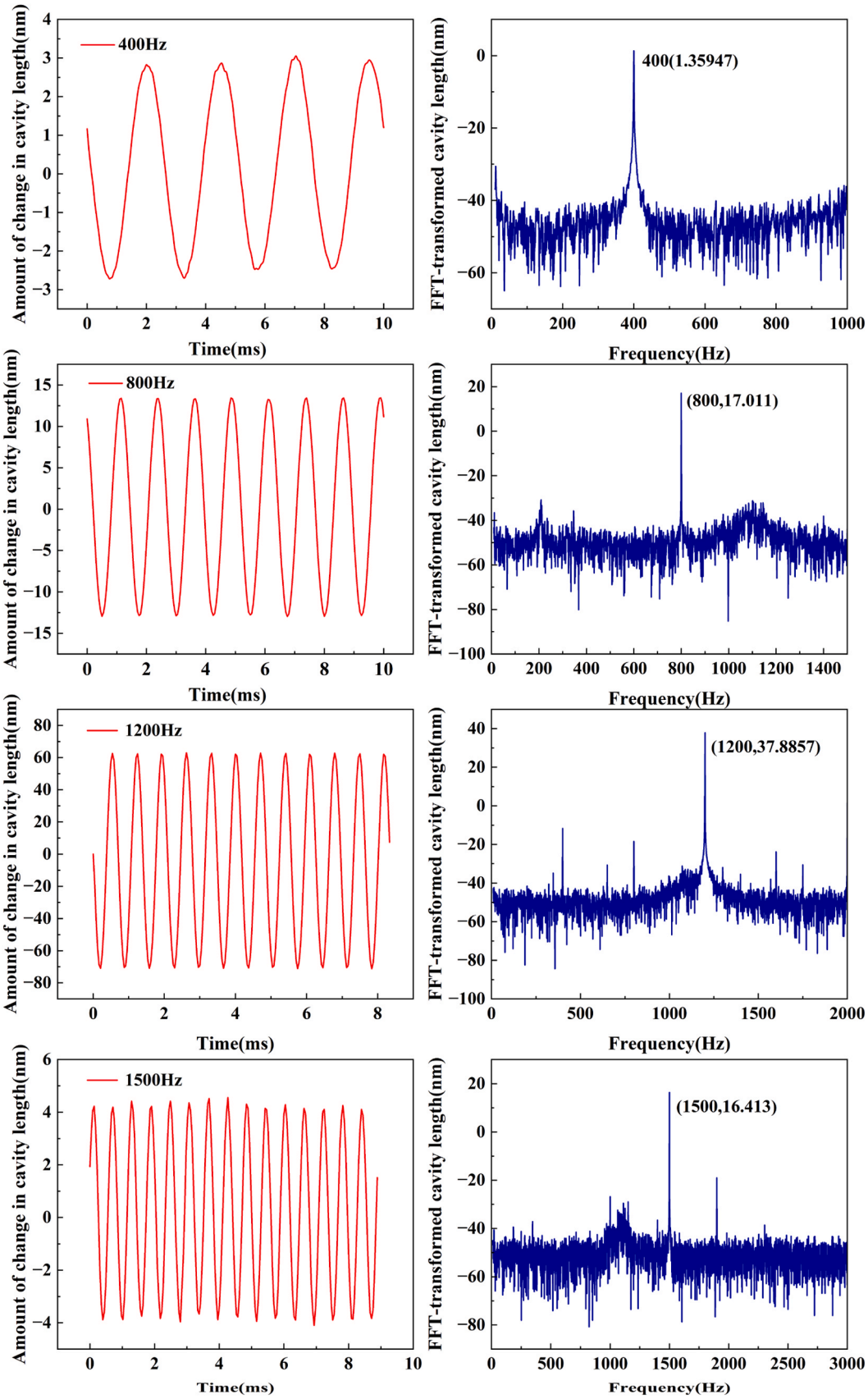

Fig. 9. The response of **FOTCS** in time domain and frequency domain at 400, 800, 1200, 1500 Hz.

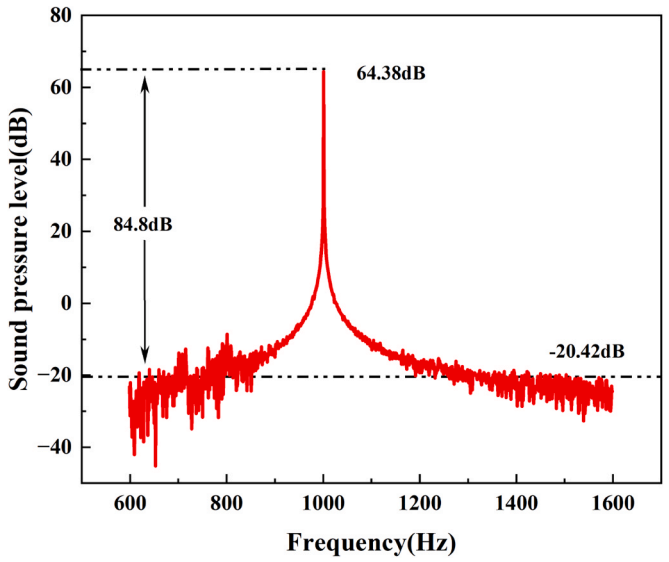

Fig. 10. Frequency spectrum of **FOTCS** at 1 kHz.

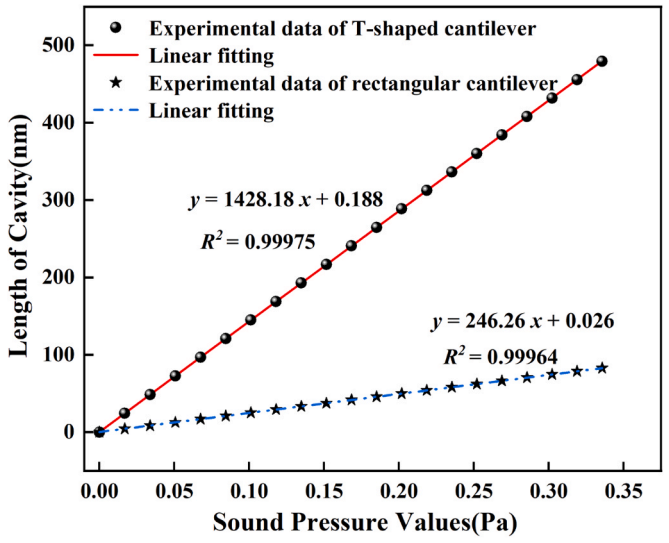

Fig. 11. Fitted curve of sound pressure sensitivity of the transducer at 1 kHz.

Table 2
Performance comparisons of F-P acoustic sensors using different material and structures.

Authors	Material	Structure	MDP
Liu *et al.* [36]	PET	Corrugated	194.42 μPa/Hz$^{1/2}$ @ 1 kHz
Xiang *et al.* [32]	Gold	Circular	95.3 μPa/Hz$^{1/2}$ @ 2 kHz
Ma *et al.* [58]	Graphene	Multilayer	60 μPa/Hz$^{1/2}$ @ 10 kHz
Yao *et al.* [59]	Polyvinyl Chloride	Circular	58.9 μPa/Hz$^{1/2}$ @ 1 kHz
Gong *et al.* [60]	Parylene-C	Circular	22.1 μPa/Hz$^{1/2}$ @ 20 Hz
Xu *et al.* [61]	Silver	Circular	14.5 μPa/Hz$^{1/2}$ @ 4 kHz
Qi *et al.* [41]	Stainless	Flywheel-like	13.06 μPa/Hz$^{1/2}$ @ 4.5 kHz
Guo *et al.* [62]	Stainless	Cantilever	5 μPa/Hz$^{1/2}$ @ 1 kHz
This work	**Stainless**	**T-Cantilever**	**1.9 μPa/Hz$^{1/2}$ @ 1 kHz**

interference spectrum. Fig. 6**(d)** illustrated the obtained interference spectrum of the T-shaped cantilever acoustic sensor, generated using an ASE source when the static cavity length was 195 μm, which clearly showed that there was a strong F-P interference between the reflected beams at the fiber end face and the inner surface of the T-shaped cantilever.

To test the resonant frequencies and sound pressure responses of the **FOTCS**, a signal generator was used to generate sinusoidal waveforms with diffent frequencies and amplitudes. Then the modulated sinusoidal waveform was transimitted to a speaker and the modulated acoutic fields in a soundproof chamber were generated using the speaker. Finally, the acoustic sensor measured the acoustic signals in the soundproof chamber, as shown in Fig. 7**.** A distributed feedback (DFB) laser beam was launched into a ring circulator and transmitted into the **FOTCS**. The reflected laser beam by the fiber tip and the T-shaped cantilever became interfered and the intensity of the interferometric signal was utilized to give the cavity length of the **FOTCS** demodulations. When the pressure was applied onto the T-shaped cantilever, the cavity length will be changed, which changed interferometric intensity. The changed intensity was detected using a photodiode (PD), which was used to record the interferometric intensity, using data capture card connected to a computer. A BK4189 microphone was used as the reference sensor and placed next to the **FOTCS** to detect the acoustic signal of the speaker, as illustrated in Fig. 7**.**

Fig. 8 showed the results of sensor's frequency responses. The sensor demonstrates a high sensitivity of 6.45 μm/Pa at its resonant frequency of 1080 Hz. Furthermore, the sensor demonstrates significant acoustic pressure responses within a frequency range of 800 Hz ~1500 Hz. These results clearly showed that it was well-suited for usages in situations which require a PAS for micro-pressure sensing applications. Fig. 9 illustrated the responses of the **FOTCS** in a time domain and a frequency domain at 400 Hz, 800 Hz, 1200 Hz and 1500 Hz, respectively. The experimental results showed that there was no distortion of the sinusoidal signal obtained from the T-shaped cantilever acoustic sensor. Fig. 10 shows that the sensor obtained an SNR value of 84.8 dB at 1 kHz, and the noise baseline was −20.42 dB for a 5 Hz resolution bandwidth. The MDP of the corresponding noise limit was 1.9 μPa/Hz$^{1/2}$.

There was a narrow frequency bandwidth near such the resonant frequency of T-shaped cantilever acoustic sensor. In other words, the **FOTCS** has a great potential to detect acoustic signals at a certain frequency range which can meet the stringent requirements of PAS gas detection systems. The acoustic pressure was further adjusted by changing the output voltage amplitudes of the singal generator. Fig. 11 showed the obtained cavity lengths of the **FOTCS** as the sound pressure was applied from 0 Pa to 0.35 Pa, revealing an excellent linear response between the cavity length of the **FOTCS** and the sound pressure. At the freqeuncy of 1 kHz, the obtained sensitivity of the **FOTCS** and the R^2 linear fitting value were 1428 nm/Pa and 0.99975, respectively. By comparison, for a conventional and rectangular cantilever with the same length (3.3 mm) the fitted value of its sensitivity at 1 kHz is only 246 nm/Pa. This clearly indicated that the sensitivity of **FOTCS** was much higher than that of the rectangular cantilever at lower frequency bands.

Table 2 summarizes performance comparisons for the F-P acoustic sensors from our work and others from the literature. The optimal sensitivity of the rectangular cantilever in the refer [60] was 211.2 nm/Pa, and the sensitivity of the T-shaped cantilever was about seven times higher when the same stainless steel material was used. The sensitivity of our proposed T-shaped acoustic sensor could be further improved if we can use silicon or other semiconductor materials, and with such mass production and low-cost processes, we believe that our proposed T-shaped acoustic sensor should have much wide-range applications in the field of PAS.

To demonstrate our proposed acoustic sensor for gas detection applications, the PA signals were measured using the fabricated FOTCS, which was put in the middle of the resonant PA cell that worked in the

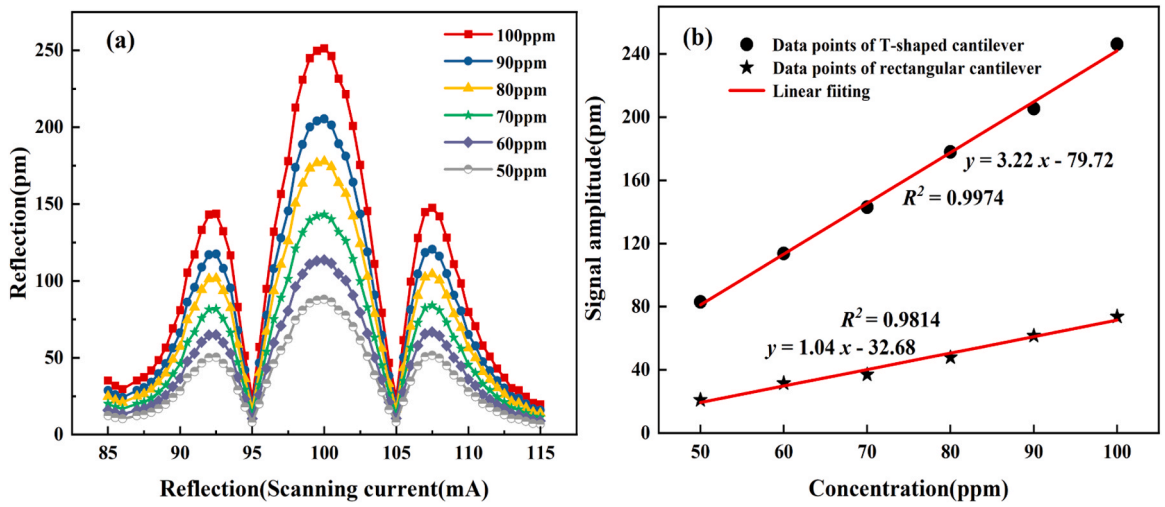

Fig. 12. (a) The 2*f*-signals of different concentrations at 100–50 ppm using **FOTCS**. (b) The linear fitting of the amplitude of 2*f*-signals.

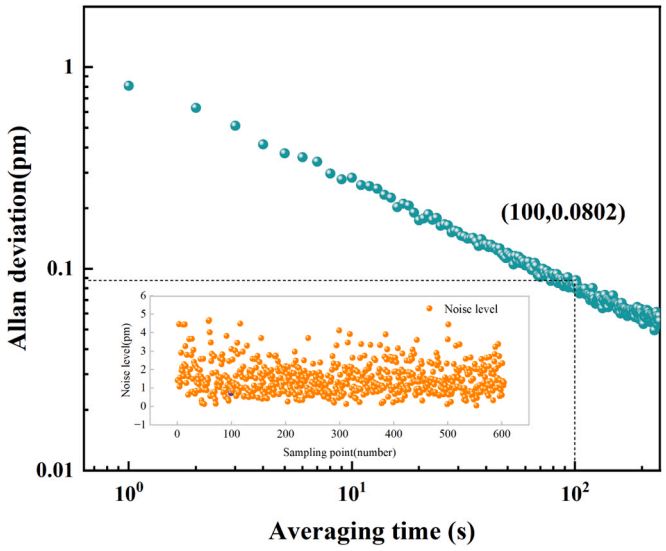

Fig. 13. Noise detection signal of the system and Allen's deviation analysis.

first resonance mode(980 Hz). The structure of the photoacoustic cell was a three-step cylindrical nesting [63], and detailed dimensional parameters were consistent with the reference.We used the DFB laser (PL-DFB-1532.5-B-A81-SA) and the modulated frequency was set at 490 Hz. The EDFA (Shanghai B&A Technology CO., LTD) was used to amplify the intensity of DFB laser, and the amplified power was 800 mW. The ratios between the C_2H_2/N_2 gas mixture and pure nitrogen (N_2) were regulated using two mass flow controllers, with N_2 gas employed as the diluent to achieve varying concentrations of C_2H_2. Then C_2H_2 with different concentrations (from 50 ppm to 100 ppm) were filled into the system. All experiments were conducted at 20 ℃ (293.15 K) and one atmospheric pressure. Changes in acoustic pressure in the photoacoustic cell caused the T-shaped cantilever to vibrate, which enabled the measurement of pressure. The temperature was kept constant during the experiment and the effect on the sensing head was negligible. The second harmonic *(2 f)* signals obtained at different C_2H_2 concentrations with the T-shaped cantilever acoustic sensor were shown in Fig. 12**(a)**.

Under the same experimental conditions, a rectangular cantilever with the dimension of 3.9 mm × 2 mm was used in our experiments, and the thickness was 20 μm. The intensity of 2 f signals increased as the increasing of C_2H_2 concentration, and the relationship was shown in Fig. 12 **(b)**.The sensitivity of PAS for C_2H_2 gas was 3.22 pm/ppm and the value of R^2 was 0.9974. The sensitivity of the T-shaped cantilever was approximately three times of that with the rectangular cantilever. To detect the limiting sensitivity, we passed pure nitrogen into the PA cell, Fig. 13 illustrated the noise floor of the whole system and the corresponding calculated values of the Allen deviation. When the integrated time was 100 s, the Allen deviation values for gas detection was 0.0802 pm. Combined with the sensitivity of T-shaped cantilever sensor, a minimum detection limit (MDL) was 24.91 ppb for C_2H_2 gas.

The results clearly proved that the proposed **FOTCS** has a high sensitivity and can precisely detect the C_2H_2 gases in PAS system.

4. Conclusion

In this paper, we proposed a highly sensitive fiber-optic acoustic sensor utilizing a T-shaped cantilever. The resonance frequency and sensitivity of T-shaped cantilever acoustic sensor were firstly analyzed using finite element analysis method. The lengths and widths of two cantilever segments in the vertical and horizontal directions of the T-shaped structure were optimized based on the simulations. Experimental results showed the resonant frequency of the T-shaped cantilever was 1080 Hz. When the acoustic pressure was changed from 0 to 0.35 Pa, there was a good linearity between the F-P cavity length and the pressure with an R^2 value of 0.99975. At a freqeuncy of 1.08 kHz, the sensitivity was 1.428 μm/Pa, with a MDP value of 1.9 μPa/Hz$^{1/2}$. For demonstration of its application, we combined this sensor with a PA cell to detect acetylene gas in a PAS system at a resonance frequency of 980 Hz. The sensitivity was 3.22 pm/ppm when the C_2H_2 gas concentration was ranged from 50 ppm to 100 ppm, and the MDL of the C_2H_2 gas was 24.91 ppb. The experimental results showed that the designed sensor achieved good detection accuracy. Due to its high sensitivity and easy frequency adjustment, the proposed sensor has broad application prospects in the field of narrow vocal band weak sound pressure detection, especially in the demand for trace gas detection in PAS systems.

CRediT authorship contribution statement

Richard (YongQing) Fu: Writing – review & editing, Supervision. **Wai Pang Ng:** Supervision, Conceptualization. **Richard Binns:** Supervision. **Jilong Wang:** Writing – original draft, Software, Data curation. **Qiaoyun Wang:** Formal analysis, Data curation, Conceptualization. **Xin Zou:** Software, Methodology. **Qiang Wu:** Supervision, Conceptualization. **Chongyue Yan:** Project administration, Investigation, Conceptualization. **Shunyuan Xu:** Supervision, Investigation.

Declaration of Competing Interest

The authors declare that they have no known competing financial interests or personal relationships that could have appeared to influence the work reported in this paper.

Data availability

The authors do not have permission to share data.

Acknowledgment

This work was supported by the National Natural Science Foundation of China (11404054), the Natural Science Foundation of Hebei Province (F2019501025, F2020501040), the Fundamental Research Funds for the Central Universities (2023FZD002).

References

[1] P. Prince, A. Hill, E. Piña Covarrubias, P. Doncaster, J.L. Snaddon, A. Rogers, Deploying acoustic detection algorithms on low-cost, open-source acoustic sensors for environmental monitoring, Sensors 19 (3) (2019) 553.
[2] H. Ge, W. Kong, R. Wang, G. Zhao, W. Ma, W. Chen, F. Wan, Simple technique of coupling a diode laser into a linear power buildup cavity for Raman gas sensing, Opt. Lett. 48 (8) (2023) 2186–2189.
[3] T. Liang, S. Qiao, Y. Chen, Y. He, Y. Ma, High-sensitivity methane detection based on QEPAS and H-QEPAS technologies combined with a self-designed 8.7 kHz quartz tuning fork, Photoacoustics 36 (2024) 100592.
[4] Y. Cai, J. Xiong, H. Chen, G. Zhang, A review of in-situ monitoring and process control system in metal-based laser additive manufacturing, J. Manuf. Syst. 70 (2023) 309–326.
[5] W. Chen, S. Qiao, Z. Zhao, S. Gao, Y. Wang, Y. Ma, Sensitive carbon monoxide detection based on laser absorption spectroscopy with hollow-core antiresonant fiber, Microw. Opt. Technol. Lett. 66 (1) (2024) e33780.
[6] A. Sampaolo, P. Patimisco, M. Giglio, A. Zifarelli, H. Wu, L. Dong, V. Spagnolo, Quartz-enhanced photoacoustic spectroscopy for multi-gas detection: a review, Anal. Chim. Acta 1202 (2022) 338894.
[7] D.C. Dumitras, M. Petrus, A.-M. Bratu, C. Popa, Applications of near infrared photoacoustic spectroscopy for analysis of human respiration: a review, Molecules 25 (7) (2020) 1728.
[8] X. Han, C. Li, M. Guo, X. Zhao, Z. Wang, H. Qi, K. Chen, Fiber-optic trace gas sensing based on graphite excited photoacoustic wave, Sens. Actuators B Chem. (2024) 135546.
[9] C. Li, H. Qi, X. Han, X. Zhao, Y. Zhang, J. Huang, W. Peng, K. Chen, Ultrahigh-speed phase demodulation of a Fabry–Perot sensor based on fiber array parallel spectral detection, Opt. Lett. 49 (3) (2024) 714–717.
[10] Y. Liu, S. Qiao, C. Fang, Y. He, H. Sun, J. Liu, Y. Ma, A highly sensitive LITES sensor based on a multi-pass cell with dense spot pattern and a novel quartz tuning fork with low frequency, Opto-Electron. Adv. 7 (2024) 230230.
[11] F. Wan, R. Wang, H. Ge, W. Kong, H. Sun, H. Wu, G. Zhao, W. Ma, W. Chen, Optical feedback frequency locking: impact of directly reflected field and responding strategies, Opt. Express 32 (7) (2024) 12428–12437.
[12] S. Qiao, Y. He, H. Sun, P. Patimisco, A. Sampaolo, V. Spagnolo, Y. Ma, Ultra-highly sensitive dual gases detection based on photoacoustic spectroscopy by exploiting a long-wave, high-power, wide-tunable, single-longitudinal-mode solid-state laser, Light Sci. Appl. 13 (1) (2024) 100.
[13] W. Chen, S. Qiao, Y. He, J. Zhu, K. Wang, L. Xiao, Y. Ma, Quasi-distributed quartz enhanced photoacoustic spectroscopy sensing based on hollow waveguide micropores, Opt. Lett. 49 (10) (2024) 2765–2768.
[14] J. Tiete, F. Domínguez, B. Da Silva, L. Segers, K. Steenhaut, A. Touhafi, SoundCompass: a distributed MEMS microphone array-based sensor for sound source localization, Sensors 14 (2) (2014) 1918–1949.
[15] Y. Chen, Y. Liu, Y. Li, H. Qi, Highly sensitive, flexible, stable, and hydrophobic biofoam based on wheat flour for multifunctional sensor and adjustable EMI shielding applications, ACS Appl. Mater. Interfaces 13 (25) (2021) 30020–30029.
[16] X.-X. Gao, J.-M. Cui, M.-Z. Ai, Y.-F. Huang, C.-F. Li, G.-C. Guo, An acoustic sensor based on active fiber Fabry–Pérot microcavities, Sensors 20 (20) (2020) 5760.
[17] H. Qi, G. Zhang, L. Xu, L. Yang, Z. Wang, Y. Xu, K. Chen, High-precision photoacoustic nitrogen dioxide gas analyzer for fast dynamic measurement, Anal. Chem. 96 (3) (2024) 1354–1361.
[18] C. Li, Y. Zhang, M. Guo, H. Qi, X. Zhao, K. Chen, Differential cantilever enhanced fiber-optic photoacoustic sensor for diffusion gas detection, Anal. Chem. 11 (2024) 4562–4569.
[19] C. Zhang, S. Qiao, Y. He, Y. Ma, Trace gas sensor based on a multi-pass-retro-reflection-enhanced differential Helmholtz photoacoustic cell and a power amplified diode laser, Opt. Express 32 (1) (2024) 848–856.
[20] W. Chen, S. Qiao, Y. He, J. Zhu, K. Wang, L. Qi, S. Zhou, L. Xiao, Y. Ma, Mid-infrared all-fiber light-induced thermoelastic spectroscopy sensor based on hollowcore anti-resonant fiber, Photoacoustics 36 (2024) 100594.
[21] C. Fang, T. Liang, S. Qiao, Y. He, Z. Shen, Y. Ma, Quartz-enhanced photoacoustic spectroscopy sensing using trapezoidal-and round-head quartz tuning forks, Opt. Lett. 49 (3) (2024) 770–773.
[22] Z. Lang, S. Qiao, T. Liang, Y. He, L. Qi, Y. Ma, Dual-frequency modulated heterodyne quartz-enhanced photoacoustic spectroscopy, Opt. Express 32 (1) (2024) 379–386.
[23] A. Rovera, A. Tancau, N. Boetti, M.D.L. Dalla Vedova, P. Maggiore, D. Janner, Fiber optic sensors for harsh and high radiation environments in aerospace applications, Sensors 23 (5) (2023) 2512.
[24] N. Wang, J.B. Fu, X.X. Li, Theoretical analysis of a new intrinsic Fabry-Perot interferometric fiber pressure sensor structure, Appl. Mech. Mater. 331 (2013) 303–306.
[25] G. Wu, H. Li, H. Ye, Z. Gong, J. Ma, M. Guo, K. Chen, W. Peng, Q. Yu, L. Mei, Ultra-high-sensitivity, miniaturized fabry-perot interferometric fiber-optic microphone for weak acoustic signals detection, Sens. (Basel) 22 (18) (2022) 6948.
[26] K. Chen, Y. Chen, B. Zhang, L. Mei, M. Guo, H. Deng, S. Liu, F. Ma, Z. Gong, Q. Yu, Highly sensitive photoacoustic microcavity gas sensor for leak detection, Sens. (Basel) 20 (4) (2020) 1164.
[27] H. Moradi, P. Parvin, A. Ojaghloo, F. Shahi, Ultrasensitive fiber optic Fabry Pérot acoustic sensor using phase detection, Measurement 172 (2021) 108953.
[28] J. Sun, L. Yan, C. Jiang, Y. Wang, Y. Lu, Y. Zhang, T. Wang, P. Chen, Highly sensitive Fabry-Perot acoustic sensor based on optic fiber spherical end surface, Opt. Fiber Technol. 80 (2023) 103440.
[29] L. Wu, Y. Zheng, C. Xue, J. Bai, J. Chen, An optical acoustic detection system based on Fabry Pérot etalon stability structure, Micromachines 12 (12) (2021) 1564.
[30] Z. Lang, S. Qiao, Y. Ma, Fabry–Perot-based phase demodulation of heterodyne light-induced thermoelastic spectroscopy, Light.: Adv. Manuf. 4 (3) (2023) 233–242.
[31] Y. Ma, T. Liang, S. Qiao, X. Liu, Z. Lang, Highly sensitive and fast hydrogen detection based on light-induced thermoelastic spectroscopy, Ultra Sci. 3 (2023) 0024.
[32] Z. Xiang, W. Dai, W. Rao, X. Cai, H. Fu, A gold diaphragm-based fabry-perot interferometer with a fiber-optic collimator for acoustic sensing, IEEE Sens. J. 21 (16) (2021) 17882–17888.
[33] S.E. Hayber, T.E. Tabaru, S. Keser, O.G. Saracoglu, A simple, high sensitive fiber optic microphone based on cellulose triacetate diaphragm, J. Light. Technol. 36 (23) (2018) 5650–5655.
[34] Y. Sun, Z. Dong, Z. Ding, N. Wang, L. Sun, H. Wei, G.P. Wang, Carbon nanocoils and polyvinyl alcohol composite films for fiber-optic fabry–perot acoustic sensors, Coatings 12 (10) (2022) 1599.
[35] B. Tian, F. Zhan, F. Han, K. Li, N. Zhao, N. Yang, Z. Jiang, An optical fiber Fabry–Pérot micro-pressure sensor based on beam-membrane structure, Meas. Sci. Technol. 29 (12) (2018) 104–125.
[36] B. Liu, G. Zheng, A. Wang, C. Gui, H. Yu, M. Shan, P. Jin, Z. Zhong, Optical fiber fabry–perot acoustic sensors based on corrugated silver diaphragms, IEEE Trans. Instrum. Meas. 69 (6) (2020) 3874–3881.
[37] H. Li, H. Deng, G. Zheng, M. Shan, Z. Zhong, B. Liu, Reviews on corrugated diaphragms in miniature fiber-optic pressure sensors, Appl. Sci. 9 (11) (2019) 2241.
[38] W. Ma, Z. Shao, W. Zhang, X. Qiao, Sensitivity-enhanced fiber-optic sensor based on a drilled PDMS diaphragm for ultrasound imaging of seismic physical model, IEEE Trans. Instrum. Meas. 71 (2022) 1–6.
[39] S. Saxena, R. Sharma, B.D. Pant, Design and development of guided four beam cantilever type MEMS based piezoelectric energy harvester, Microsyst. Technol. 23 (6) (2016) 1751–1759.
[40] X. Niu, Y. Huang, L. Zhang, L. Wang, C. Hu, C. Deng, P. Wu, Y. Lu, Q. Li, Q. Zhang, X. Zhang, T. Wang, A sensitivity-enhanced fiber optic fabry-perot acoustic sensor based on grooved diaphragm, IEEE Photonics Technol. Lett. 35 (8) (2023) 422–425.
[41] X. Qi, S. Wang, J. Jiang, K. Liu, P. Zhang, Z. Li, T. Liu, Study on the sensitization effect of flywheel-like diaphragm on fiber-optic fabry-perot acoustic sensor, IEEE Access 8 (2020) 99286–99293.
[42] H. Qi, X. Zhao, Y. Xu, L. Yang, J. Liu, K. Chen, Rapid photoacoustic exhaust gas analyzer for simultaneous measurement of nitrogen dioxide and sulfur dioxide, Anal. Chem. 13 (2024) 5258–5264.
[43] X. Zhao, H. Qi, H. Wang, X. Wang, M. Guo, W. Peng, K. Chen, Dense multibutterfly spots-enhanced miniaturized optical fiber photoacoustic gas sensor, Anal. Chem. 14 (2024) 5554–5559.
[44] X. Zhao, H. Qi, Z. Wang, F. Ma, C. Li, M. Guo, K. Chen, Cantilever enhanced fiber-optic photoacoustic microprobe for diffusion detection of sulfur dioxide, Sens. Actuators B Chem. 405 (2024) 135340.
[45] Y. Ma, R. Lewicki, M. Razeghi, F.K. Tittel, QEPAS based ppb-level detection of CO and N 2 O using a high power CW DFB-QCL, Opt. Express 21 (1) (2013) 1008–1019.
[46] L. Liu, H. Huan, W. Li, A. Mandelis, Y. Wang, L. Zhang, X. Zhang, X. Yin, Y. Wu, X. Shao, Highly sensitive broadband differential infrared photoacoustic spectroscopy with wavelet denoising algorithm for trace gas detection, Photoacoustics 21 (2021) 100228.
[47] L. Liu, H. Huan, A. Mandelis, L. Zhang, C. Guo, W. Li, X. Zhang, X. Yin, X. Shao, D. Wang, Design and structural optimization of T-resonators for highly sensitive photoacoustic trace gas detection, Opt. Laser Technol. 148 (2022) 107695.
[48] L. Liu, H. Huan, X. Zhang, L. Zhang, X. Shao, A. Mandelis, L. Dong, Laser induced thermoelastic contributions from windows to signal background in a photoacoustic cell, Photoacoustics 22 (2021) 100257.
[49] L. Zhang, L. Liu, X. Zhang, X. Yin, H. Huan, H. Liu, X. Zhao, Y. Ma, X. Shao, T-type cell mediated photoacoustic spectroscopy for simultaneous detection of multi-

component gases based on triple resonance modality, Photoacoustics 31 (2023) 100492.
[50] M. Guo, K. Chen, B. Yang, C. Li, B. Zhang, Y. Yang, Y. Wang, C. Li, Z. Gong, F. Ma, Q. Yu, Ultrahigh Sensitivity Fiber-Optic Fabry–Perot Interferometric Acoustic Sensor Based on Silicon Cantilever, IEEE Trans. Instrum. Meas. 70 (2021) 1–8.
[51] Ö. Civalek, Ç. Demir, Bending analysis of microtubules using nonlocal Euler–Bernoulli beam theory, Appl. Math. Model. 35 (5) (2011) 2053–2067.
[52] S. Tian, Y. Qiao, M. Liang, M. Feng, Y. Gao, L. Li, C. Shan, Sensitivity-enhanced Fabry-Perot interferometric fiber-optic microphone using hollow cantilever, Opt. Express 31 (13) (2023) 21796–21805.
[53] K. Chen, H. Deng, M. Guo, C. Luo, S. Liu, B. Zhang, F. Ma, F. Zhu, Z. Gong, W. Peng, Tube-cantilever double resonance enhanced fiber-optic photoacoustic spectrometer, Opt. Laser Technol. 123 (2020) 105894.
[54] K. Mohamed, H. Elgamal, S.A. Kouritem, An experimental validation of a new shape optimization technique for piezoelectric harvesting cantilever beams, Alex. Eng. J. 60 (1) (2021) 1751–1766.
[55] C. Zhang, Q. Wang, H. Pan, F. Pian, Z. Li, P. Shan, Highly sensitive multi-pass enhanced photoacoustic cell based on three spot-ring structure (TSR-MPC), Infrared Phys. Technol. 118 (2021) 103880.
[56] Y. Ma, S. Qiao, Y. He, Y. Li, Z. Zhang, X. Yu, F.K. Tittel, Highly sensitive acetylene detection based on multi-pass retro-reflection-cavity-enhanced photoacoustic spectroscopy and a fiber amplified diode laser, Opt. Express 27 (10) (2019) 14163–14172.
[57] K. Chen, Z. Gong, M. Guo, S. Yu, C. Qu, X. Zhou, Q. Yu, Fiber-optic Fabry-Perot interferometer based high sensitive cantilever microphone, Sens. Actuators A: Phys. 279 (2018) 107–112.
[58] J. Ma, H. Xuan, H.L. Ho, W. Jin, Y. Yang, S. Fan, Fiber-optic Fabry–Pérot acoustic sensor with multilayer graphene diaphragm, IEEE Photonics Technol. Lett. 25 (10) (2013) 932–935.
[59] Q. Yao, X. Guo, L. Xie, L. Sun, F. Yu, X. Zhao, A miniature Fabry–Pérot fiber interference sensor based on polyvinyl chloride membrane for acoustic pressure sensing in mid–high-frequency band, Materials 14 (24) (2021) 7605.
[60] Z. Gong, K. Chen, X. Zhou, Y. Yang, Z. Zhao, H. Zou, Q. Yu, High-sensitivity Fabry-Perot interferometric acoustic sensor for low-frequency acoustic pressure detections, J. Light. Technol. 35 (24) (2017) 5276–5279.
[61] F. Xu, J. Shi, K. Gong, H. Li, R. Hui, B. Yu, Fiber-optic acoustic pressure sensor based on large-area nanolayer silver diaghragm, Opt. Lett. 39 (10) (2014) 2838–2840.
[62] K. Chen, Z. Yu, Q. Yu, M. Guo, Z. Zhao, C. Qu, Z. Gong, Y. Yang, Fast demodulated white-light interferometry-based fiber-optic Fabry–Perot cantilever microphone, Opt. Lett. 43 (14) (2018) 3417–3420.

Jilong Wang received his B.S. degree in Qingdao University of Technolo China, in 2018. He is now pursuing a master's degree in control engineering from Northeastern University. His research interest is fiber optic Fabry-Perot micro pressure sensor.

Qiaoyun Wang received the B.S. degree from Tangshan Normal University in 2003, and the Ph.D. degree in Optical Engineering from the Dalian University of Technology in 2010. Dr. Wang is now an associate professor in the School of Control Engineering at Northeastern University at Qinhuangdao. Her research interests include photoacoustic spectroscopy, fiber optical sensors, infrared spectroscopy, Raman spectroscopy and acoustofluidic, and their applications.

Chongyue Yan received his B.S. degree in Yanshan University, China, in 2023. He is now pursuing a master's degree of optical engineering from Northeastern University. His research interest is fiber optic acoustic sensor based on F-P structure.

Shunyuan Xu received his B.S. degree in Yancheng Institute of Technology, China, in 2018. He is now pursuing a master's degree in control engineering from Northeastern University. His research interest is photoacoustic cell design based on photoacoustic spectroscopy.

Xin Zou received her B.S. degree in East China Jiaotong University, China, in 2018. He is now pursuing a master's degree of Control Science and Engineering from Northeastern University. His research interest is research on spectral quantitative analysis algorithm.

Qiang Wu is an Associate Professor at the Department of Mathematics, Physics & Electrical Engineering, Northumbria University at Newcastle. His current research interest lies in Photonics including the fibre Bragg grating devices, heterocore fibre structures, nonlinear effects in photonic crystal fibre and its application, and surface plasmon resonant.

Wai Pang Ng is currently Professor and Head of Department in the Department of Mathematics, Physics and Electrical Engineering. He received his BEng (Hons) in Communications and Electronic Engineering, from the University of Northumbria, U. K. and his Ph.D. in Electronic Engineering from University of Wales, Swansea. His research interests include radio-over-fiber, cognitive radio, high speed optical communications, adaptive digital signal processing and distributed fibre sensing.

Dr Richard Binns is the Head of Department of Mathematics Physics and Electrical Engineering and Associate Professor at Northumbria University. He graduated from Huddersfield University with a degree in Electronic and Information Engineering in 1993 and also a PhD in Analogue Test strategies in 1997. Current research works is varied from design of electronics for visible light communications, energy management in electric vehicles, research into radiation detection mechanisms for personal dosimetry and power control systems development.

Richard YongQing Fu is a professor in the Faculty of Engineering and Environment, University of Northumbria at Newcastle, UK. He obtained his BSc/MSc from Xian University of technology, China, and a PhD degree from Nanyang Technological University, Singapore. He has extensive experience in smart thin films/materials, biomedical microdevices, energy materials, lab-on-chip, micromechanics, MEMS, nanotechnology, sensors and microfluidics.